Contents lists available at ScienceDirect

Carbon

journal homepage: http://ees.elsevier.com

Tuning graphene doping by carbon monoxide intercalation at the Ni(111) interface

Simone Del Puppo [a], Virginia Carnevali [a,b,e], Daniele Perilli [c], Francesca Zarabara [a], Alberto Lodi Rizzini [b], Gabriele Fornasier [a,b], Erik Zupanič [d], Sara Fiori [a,b], Laerte L. Patera [a,b,f], Mirco Panighel [b], Sunil Bhardwaj [b], Zhiyu Zou [b], Giovanni Comelli [a,b], Cristina Africh [b], Cinzia Cepek [b], Cristiana Di Valentin [c], Maria Peressi [a,*]

[a] *Department of Physics, University of Trieste, via A. Valerio 2, I-34127, Trieste, Italy*
[b] *CNR-IOM, Laboratorio TASC, S.S. 14 Km 163.5, Basovizza, I-34149, Trieste, Italy*
[c] *Department of Materials Science, University of Milano-Bicocca, via R. Cozzi 55, I-20125 Milano, Italy*
[d] *Jožef Stefan Institute, Jamova 39, SI-1000 Ljubljana, Slovenia*
[e] *Central Michigan University, Mount Pleasant, MI, 48858, USA*
[f] *Department of Chemistry, Technical University of Munich, Lichtenbergstraße 4, 85748, Garching, Germany*

ARTICLE INFO

Article history:
Received 25 September 2020
Received in revised form 31 December 2020
Accepted 15 January 2021
Available online xxx

Keywords
Graphene
Graphene-substrate interface
Carbon monoxide
Intercalation
Doping

ABSTRACT

Under near-ambient pressure conditions, carbon monoxide molecules intercalate underneath an epitaxial graphene monolayer grown on Ni(111), getting trapped into the confined region at the interface. On the basis of *ab-initio* density functional theory calculations, we provide here a full investigation of the intercalated CO pattern, highlighting the modifications induced on the graphene electronic structure. For a CO coverage as low as 0.14 monolayer (ML), the graphene layer is spatially decoupled from the metallic substrate, with a significant C 1s core level shift towards lower binding energies. The most relevant signature of the CO intercalation is a clear switching of the graphene doping state, which changes from n-type, when strongly interacting with the metal surface, to p-type. The shift of the Dirac cone linearly depends on the CO coverage, reaching about 0.9 eV for the saturation value of 0.57 ML. Theoretical predictions are compared with the results of scanning tunnelling microscopy, low-energy electron diffraction and photoemission spectroscopy experiments, which confirm the proposed scenario for the nearly saturated intercalated CO system. This result opens the way to the application of the graphene/Ni(111) interface as gas sensor to easily detect and quantify the presence of carbon monoxide.

1. Introduction

Nickel is an optimal substrate for graphene (Gr) growth via Chemical Vapor Deposition (CVD), since its excellent lattice match with the carbon network ensures the formation of high-quality flakes, with the drawback of a strong interaction which leads to the loss of free-standing Gr features. Intercalation of atoms or molecules can be exploited to modify at will the electronic properties of Gr and to decouple it from the substrate [1–7]. In this framework, intercalation of carbon monoxide (CO) is particularly relevant, since CO is one of the simplest and most harmful molecules in atmosphere, and a system for its trapping can be of potential application as sensor or catalytic reactor.

The adsorption of CO on bare metal surfaces has been widely studied by means of different experimental techniques and numerical simulations. On Ni(111) four different high symmetry adsorption sites are available, namely top, bridge, hollow hcp and hollow fcc. There is consensus that the adsorption on hollow sites is favored at low coverage, when the molecule-substrate interaction dominates [8,9], but the situation is not as clear at higher coverages, where lateral intermolecular interactions play a relevant role.

A regular pattern with $c(4\times2)$ periodicity is revealed for a coverage of 0.5 monolayer (ML) by Low Energy Electron Diffraction (LEED) [10], Surface-Extended X-Ray Absorption Fine Structure (SEXAFS) [11], LEED I–V [12], Scanning Tunnelling Microscopy (STM) [13] experiments and supported by Density Functional Theory (DFT) calculations [14]. This pattern can also be described by a smaller $\left(2\times\sqrt{3}\right)$ cell where only one or at most two types of sites are occupied [11,15,16]. The hollow sites are indicated as the preferred ones by most of the literature, but alternative suggestions for bridge sites only [17] or a mixture of bridge and top sites have been put forward from Infrared Reflection Absorption Spectroscopy (IRAS), STM [16] and Sum Frequency Generation (SFG) experiments [17] (in the latter work, also for other coverages). Temperature Programmed Desorption (TPD) and IRAS suggest that the site occupation depends also on the temperature: whereas hollow sites are preferentially occupied below 100 K, conversion towards the top sites occurs at higher temperatures [18].

The saturation coverage of 0.57 monolayer (ML), is unanimously described using a rhombic $(\sqrt{7}\times\sqrt{7})R19.1^{\circ}$ pattern [19–21], for which

* Corresponding author.
E-mail address: peressi@units.it (M. Peressi)

https://doi.org/10.1016/j.carbon.2021.01.120
0008-6223/

X-ray photoemission spectroscopy (XPS) suggests the occupation of top and bridge sites [20].

The scenario, already quite complicated, becomes even less clear when CO is trapped at the Gr/Ni(111) interface, where no direct information concerning the adsorption sites is yet available from experimental investigations. Wei et al. investigated the CO intercalation/de-intercalation at the Gr/Ni(111) interface in the mbar regime by XPS [22], demonstrating that high CO pressure is needed for its adsorption in between Gr and Ni. Perilli et al. have recently shown that the presence of N-dopants in Gr highly facilitates the permeation process and proposed a comprehensive explanation of the intercalation mechanism [23]. However, a detailed description of the adsorption pattern of the trapped CO is still lacking, as well as of its effect on the Gr electronic structure.

Here we provide a full characterization of the CO intercalation pattern at the interface between Gr and Ni(111) and a detailed description of the changes induced in the Gr electronic structure by combining LEED, XPS, STM experiments and DFT calculations. We mainly focus on high CO coverages, 0.50 ML and 0.57 ML, but we extend the theoretical investigation also to a coverage as low as 0.14 ML. In the whole investigated range, we find that carbon monoxide spatially decouples graphene from the substrate, yielding STM images which are undistinguishable from non-interacting Gr. However, the intercalated CO layer deeply affects the Gr electronic structure, and, in particular, the position of the restored Dirac cone and the C 1s core level binding energies.

2. Methods

2.1. Experimental methods

Pristine Gr was prepared in an ultra-high vacuum (UHV) chamber with a base pressure of $\sim 2 \times 10^{-10}$ mbar. The Ni(111) single crystal was cleaned by several cycles of Ar^+ sputtering at 1.5 kV at room temperature (RT) and annealing at 600 °C, for a few minutes. Standard Gr growth was performed in UHV by low-pressure CVD, using ethylene (C_2H_4) as precursor. LEED and STM characterization was performed in UHV in order to assess the quality and homogeneity of the as-grown Gr sample.

CO reactivity experiments have been carried out *in-situ*, in a home-made high-pressure cell with a base pressure of $\sim 10^{-8}$ mbar, operating in flow mode. For the high-pressure treatments, CO (SIAD, purity: N3.7) was used without further purification. Pressures in the high-pressure cell were measured with a commercial pressure gauge placed inside the cell.

STM measurements were performed in UHV at room temperature with an Omicron variable-temperature STM. All topographic images were acquired in constant-current mode. STM images were analyzed with the Gwyddion software package [24], after applying moderate noise filtering. Crystallographic orientation of the images was determined by combining LEED measurements with the analysis of the epitaxial structure formed by pristine Gr on the Ni(111) surface, as described in Ref. [25].

Photoemission experiments were performed both *in-situ* and ex-*situ* in a dedicated UHV system with a base pressure in the range of 10^{-9} mbar. Before the *ex-situ* measurements, the sample was shortly flashed to 390 K to remove contaminants. All the spectra were collected at RT in normal emission geometry using a hemispherical electron energy analyzer, a conventional non monochromatic Mg $K_{\alpha 1,2}$ X-ray source for XPS ($h\nu = 1253.6$ eV) and a He discharge lamp for He II UPS ($h\nu = 40.8$ eV), with an overall experimental energy resolution of ~0.8 eV and ~0.1eV, respectively. All binding energies were calibrated by measuring the Fermi level. The XPS spectra were analyzed by performing a non-linear least squares fit of the data. We used a Shirley background and Doniach-Sunjic lineshapes for the C 1s peaks. In the fitting procedure, for the C 1s spectra, we used the four components already identified in our previous work on the Gr on Ni(111) system [26], with the addition of two new components related to the presence of intercalated CO. Overall, up to six components were included, corresponding to: i) C atoms in the graphene layer detached from Ni by CO intercalation; ii) C atoms in the graphene layer directly interacting with Ni(111); iii) C atoms in a free-standing-like graphene layer (non-interacting graphene with Ni(111) due to presence of carbide at the interface); iv) C atoms of CO molecules adsorbed on Ni(111) in bridge and fcc/hcp positions (as discussed later); v) C atoms of CO molecules adsorbed on Ni(111) in top position; and vi) C atoms in nickel carbide [22,26]. In the fitting procedure we fixed the binding energies of iii) and vi) to literature values, i.e. 284.4 eV and 283.2 eV, respectively [22,26]. All the other binding energies were allowed to vary within energy ranges not overlapping to each other, starting from the values predicted by DFT calculations. Because of the limited energy resolution, the C 1s peaks corresponding to CO in bridge and fcc/hcp position, which are expected to lie very close to each other, were merged into a single peak (component iv). The asymmetry parameter was fixed to 0.12 for all the graphene related C 1s components, to 0.09 for carbide and to zero for all the CO-related components [26]. All the Lorentzian widths were fixed to 0.25 eV [26], while all the intensities and Gaussian widths were free fittings parameters. The O 1s spectrum after *in situ* CO intercalation was analyzed using two symmetric components, corresponding to CO in top and bridge position, in agreement with literature [22].

2.2. DFT simulations

Most of the DFT calculations were performed with Quantum ESPRESSO (QE) code [27], using plane-wave basis set and the Generalized Gradient Approximation for the exchange-correlation functional in the Perdew-Burke-Ernzerhof parametrization (GGA-PBE) [28]. Ultrasoft, scalar-relativistic pseudopotentials with non-linear core corrections from the QE website have been used [29]. In order to describe the graphene/Ni(111) interaction, semi-empirical corrections accounting for the van der Waals interactions were included with the DFT-D2 approach [30]. The results discussed in the main text, including those concerning CO adsorption on Ni in the absence of Gr capping, always make use of this correction. Convergence tests suggested a kinetic energy cutoff of 30 Ry for the plane-wave basis set. The equilibrium lattice parameters characterizing the clean Ni(111) surface and the free-standing Gr are 2.49 Å and 2.46 Å respectively, equal to the experimental values. We have kept the lattice parameter of Ni to simulate the slab and accommodated the Gr overlayer accordingly.

We used periodically repeated supercells with slab geometries, with 3 Ni layers and Gr adsorbed on one side and a vacuum spacing of about 24 Å between Gr and the parallel consecutive Ni(111) surface. We always consider epitaxial graphene, i.e., aligned with respect to the substrate, and in particular in the top-fcc registry as initial configuration, motivated by the higher abundance of such domains as experimentally detected [31]. The periodic cells have different shapes and sizes in the plane to cope with the different CO coverages and accommodate different ordered patterns both for adsorption on clean Ni, in the absence of Gr capping (Figs. S1, S2, S3), and for intercalation at the Gr/Ni interface (Figs. S4, S5, S6). Specifically, we use a rhombic $(\sqrt{7} \times \sqrt{7})R19.1°$ cell for 0.14 ML and 0.57 ML (Figs. S1, S3, S4, S6), rectangular $\left(2 \times \sqrt{3}\right)$ and parallelogrammatic $c(4 \times 2)$ cell for 0.50 ML (Figs. S2 and S4). All the atomic positions are optimized, apart from the bottom metallic layer, minimizing the forces acting on each atom. The intercalated molecules are initially slightly displaced from perfectly symmetric geometries (high symmetry adsorption sites and orientation perpendicular to the surface) in order to ease the search for global minima and to avoid trapping of the system in metastable configurations.

Concerning the Brillouin zone sampling, Monkhorst-Pack k-point meshes [32] with similar density for the different cells have been used, namely: 6 × 6 × 1 for the $(\sqrt{7}\times\sqrt{7})R19.1^\circ$ cell, 9 × 9 × 1 for the $c(4\times2)$ cell and 6 × 6 × 1 for the $\left(2\times\sqrt{3}\right)$ cell for the structural optimization and self-consistent calculations; 48 × 48 × 1 and 72 × 72 × 1 for the $(\sqrt{7}\times\sqrt{7})R19.1^\circ$ cell and for the $c(4\times2)$ cell, respectively, for the non-self-consistent calculations for the projected density of states (PDOS). The Methfessel-Paxton smearing technique with an energy broadening of 0.01 Ry has been adopted [33].

CO vibrational modes were calculated by diagonalizing the dynamical matrix at Γ point only and treating all CO degrees of freedom within the harmonic oscillator approximation.

Absolute values of the core-level binding energies (BE) are not accessible in the pseudopotential formalism, where only their differences (i.e., core level shifts, CLS) are meaningful [34,35]. To this purpose, we used the final state approximation. A *1s* core-excited pseudopotential was generated for C, substituting in the simulation cell one C atom at the time. For calculations with core-excited atoms, the plane-wave energy cutoff was increased to 50 Ry for the wavefunctions and 350 Ry for the charge density. The CLS between two configurations *i* and *j* with a different core-excited C atom is given by:

$$CLS(j-i) = E_{tot}(j^*) - E_{tot}(i^*) - \left[E_{tot}(j) - E_{tot}(i)\right]$$

where $E_{tot}(i^*)$, $E_{tot}(j^*)$ are the ground state total energies of the configurations i* and j* with one core-exited C atom, and $E_{tot}(i)$, $E_{tot}(j)$ are the ground state total energies of the configurations *i* and *j* with no core-excited atoms, respectively. If the CLS is calculated for two different positions of the core-excited atom in the same configuration, the total energy of the ground state configuration before excitation is the same, and the term in square brackets vanishes. In order to avoid interactions between repeated images of core-excited atoms, we have used the same large simulation cells used for the CO intercalation also for core-excited calculations of an individual C atom in free standing Gr or Gr/Ni system without CO capping. For comparison with the experimental data, all the calculated CLS have been referred to the free-standing Gr, aligning the experimental and calculated binding energies.

Stick-and-ball models and charge transfer plots were rendered with the XCrysDen [36] and VMD [37] software.

STM simulations (shown in Fig. S10 in Supplementary Data) were performed using the Tersoff-Hamann approach [38], according to which the tunnelling current is proportional to the Integrated Local Density of States (ILDOS). The energy integration was performed in an energy window corresponding to the bias voltage used in the experiments. The ILDOS was plotted on a plane parallel to Gr to simulate the constant height mode. STM images were drawn with the Gwyddion software [24].

3. Results and discussion

3.1. Experimental results

Graphene was grown by low-pressure CVD on a clean Ni(111) substrate, keeping the sample at 600 °C and dosing C_2H_4 at p = 2 × 10^{-7} mbar, typically for 60 min. LEED and STM measurements, performed *in-situ* under UHV conditions, indicate the formation of high-quality epitaxial Gr, typically adopting the most common top-fcc registry with the substrate [31]. As previously reported [23], after dosing CO with a pressure in the 500 mTorr–10 Torr range for at least one hour, large areas of graphene, showing the full hexagon characteristic of decoupled flakes, are imaged by STM (Fig. 1a; comparison with a simulated STM image in Fig. S10). LEED shows new additional spots, beside those related to Ni and Gr, which are compatible with the co-existence of c(4 × 2) and $(\sqrt{7}\times\sqrt{7})$R19.1° CO domains, with a local coverage of 0.5 ML and 0.57 ML respectively, in line with previous results obtained in the absence of Gr capping [19–21]. In particular, Fig. 1b presents the LEED pattern of an intercalated sample where c(4 × 2) domains predominate. In summary, STM and LEED provide information about the periodicity of the intercalated CO pattern, but no indication about the specific adsorption sites. In order to clarify the latter issue, we performed XPS experiments *ex situ* from the same layer used for STM and LEED experiments (Fig. 2, bottom spectrum). Several components, listed in Table S2, contribute to the observed C 1s lineshape. Three of them are the well-known components previously observed in the Gr on Ni(111) system: strongly interacting graphene at 284.8 eV (green), non-interacting graphene at 284.4 eV (violet), accompanied by

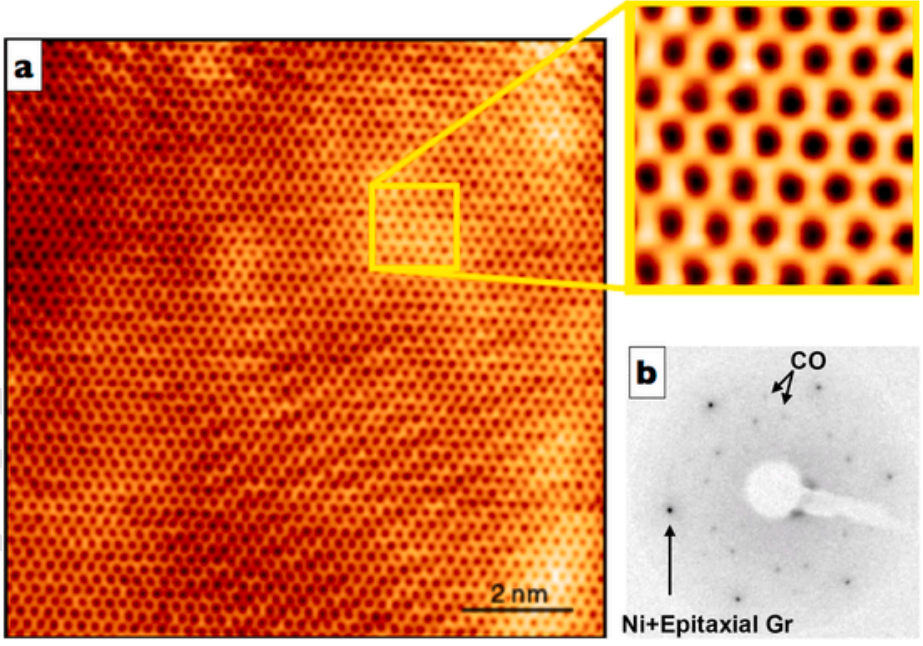

Fig. 1. (a) STM image of graphene/Ni(111) after CO intercalation [I = 1 nA, V_b = 0.2 V; inset: 1.5 × 1.5 nm^2, I = 1 nA, V_b = 0.4 V]. (b) LEED pattern at 100 eV of graphene/Ni(111) after CO intercalation (10 min @ 10 Torr). (A colour version of this figure can be viewed online.)

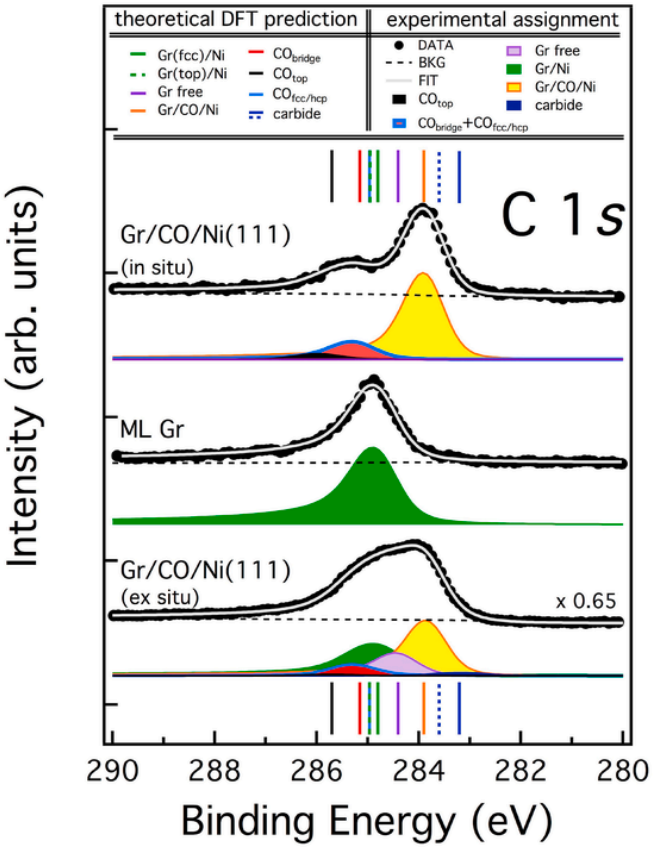

Fig. 2. Comparison of the experimental XPS spectrum and the calculated binding energies of C 1s core level for Gr/CO/Ni (bottom panel: *ex situ*; upper panel: *in situ*) and for epitaxial Gr/Ni (middle panel). The experimental spectrum of Gr/CO/Ni detected *ex situ* (same sample as in Fig. 1(b)) has been deconvoluted with six components. Only three of them contribute to the intercalated layer prepared *in situ*. The DFT calculated values correspond to the configuration with 0.50 ML of CO (which is the coverage characterizing the experimental sample), except for the values for CO in bridge and in top positions which are shown as a reference and are calculated in an artificial configuration at 0.14 ML with constraints on the in-plane position of CO. See Table S2 and Fig. S7 for details. (A colour version of this figure can be viewed online.)

the fingerprint of the underlying surface carbide at 283.2 eV (dark blue). In addition, intercalation brings in three new components: the main peak at 283.8 eV (yellow), a peak at 285.3 eV (red/blue) and a very small feature at 285.9 eV (black).

In order to achieve a safe identification of the peaks, considering the complexity of the spectrum, it is crucial to rule out possible artefacts introduced by *ex-situ* contamination. We thus repeated the XPS measurements on a new intercalated layer prepared *in-situ*. This time the starting Gr layer was purely epitaxial (middle spectrum in Fig. 2), with a single peak (green) at 284.8 eV, corresponding to strongly interacting graphene. The structure of the XPS spectrum after intercalation (top curve in Fig. 2) is much simpler. First of all, since there are no rotated Gr domains with carbide underneath, the violet and blue components are missing. Furthermore, as the intercalation was carried out *in situ*, no loss of interfacial CO took place, so that the strongly interacting component (green) is absent too. The three remaining components are in excellent agreement with the corresponding ones in the *ex situ* spectrum, supporting their correlation to intercalated CO. In particular, the main yellow peak can be safely attributed to Gr decoupled from the Ni surface by the intercalated CO layer.

The presence of CO on the Ni surface is confirmed also by the O 1s spectrum measured from the same *in situ* preparation (Fig. S11), very similar to corresponding spectra for CO on Ni(111) [26].

By analysing the peaks' intensity, taking into account also the attenuation due to the presence of the Gr layer [25,26], it is possible to deduce the CO coverage in the different preparations, obtaining an estimated coverage of 0.6 ± 0.1 ML. This is consistent, within uncertainties, with both the coverages expected for the c(4 × 2) and $(\sqrt{7} \times \sqrt{7})R19.1^{\circ}$ CO domains, respectively 0.5 ML and 0.57 ML.

Finally, in order to obtain information about the electronic structure of the intercalated layers close to the Fermi level, we measured the valence band photoemission spectra, which are shown in Fig. S12.

3.2. DFT simulations

In order to rationalize the specific CO intercalation pattern and the observed effects on the electronic structure, we performed a systematic density functional theory investigation of Gr/CO/Ni(111) for the experimentally observed CO concentrations of 0.57 ML and 0.50 ML, as well as for 0.14 ML. For the sake of comparison and validation of our results, it is useful to shortly examine first the CO adsorption patterns on Ni(111), in the absence of Gr capping and for the same coverages, although already studied in literature.

3.2.1. CO/Ni(111)

In all cases, the optimized structures are characterized by CO molecules almost perpendicular to the surface, with the C end down (Figs. S1, S2, S3). We calculated the adsorption energy as:

$$E_{ads\ CO} = \frac{1}{N_{CO}} \left(E_{CO/Ni} - E_{Ni} - N_{CO} * E_{CO}\right)$$

where $E_{CO/Ni}$is the total energy of the CO/Ni(111), E_{Ni} is the energy of the corresponding clean Ni slab, E_{CO} is the energy of a gas-phase CO molecule and N_{CO} is the number of CO molecules adsorbed on the slab.

At low coverage (θ = 0.14 ML), hollow (fcc, hcp) adsorption sites are favored, but also bridge, and, to a lesser extent, top sites are stable, with adsorption energies per CO molecule ranging from −2.24 eV (hollow hcp) to −1.86 eV (top) (Fig. S1 and Table S1).

At a coverage of 0.50 ML, almost uniformly equispaced CO molecules can be arranged in both $\left(2 \times \sqrt{3}\right)$ and $c\,(4 \times 2)$ patterns. The most stable pattern $\left(2 \times \sqrt{3}\right)$ involves CO molecules alternatively in hollow fcc and hcp sites (configuration A in Fig. S2), with an average adsorption energy of −2.26 eV per molecule. The $c\,(4 \times 2)$ cell (configuration B in Fig. S2) involves instead top sites and "hybrid" sites, which are intermediate between fcc and bridge, and between hcp and bridge. For this configuration, the average adsorption energy is −1.98 eV, lower than in configuration A, as expected since the top site is the least favored.

A coverage of 0.57 ML cannot be accommodated in a commensurate pattern of regularly distributed perfectly high-symmetry sites. Three different stable configurations, shown in Fig. S3, are found, all involving CO molecules mainly in hollow sites (both fcc and hcp), but slightly displaced from high symmetry positions towards top and bridge sites. The average adsorption energy is very similar, between −2.15 eV and −2.16 eV. Two of these configurations are similar to those proposed in Ref. [14].

To summarize, we find a variation of about 0.4 eV, at most, for the average CO adsorption energy within the explored coverage range; larger differences are related to the occupation of less favored adsorption sites rather than to repulsive intermolecular interaction. Our results are in agreement with the literature, taking into account the different details of the calculations.

3.2.2. Gr/CO/Ni(111)

3.2.2.1. Structures In the study of CO intercalated at the Gr/Ni(111) interface, we consider Gr initially aligned in the top-fcc registry with respect to the underlying Ni(111) surface, and allow the structures to fully relax. Remarkably, even for the smallest coverage (0.14 ML), the Gr layer is well detached from the Ni surface, increasing its original distance (2.12 Å without CO) to 5.52 Å, while maintaining the top-fcc registry. In the optimized structures, the CO molecules are almost perpendicular to the surface, as in the absence of Gr capping. For 0.14 ML, only hollow (fcc, hcp) sites are stable CO adsorption sites (Fig. S4). For comparison, the intercalation energy for top and bridge sites has been calculated by constraining the in-plane position of CO. Gr capping clearly puts a constraint for the adsorbed CO pattern also at higher coverage: at 0.50 ML, only one pattern is found, with the occupation of fcc and hcp sites (Fig. S5), corresponding to configuration A of Fig. S2, without Gr. The scenario for 0.57 ML is very rich. Three different adsorption patterns are found, characterized mostly by the occupancy of hollow sites with CO molecules slightly displaced towards top and bridge sites, similarly to the case without Gr capping (Fig. S6). Out of the 4 CO molecules included in the ($\sqrt{7} \times \sqrt{7}$) R19.1° simulation cell, one configuration shows 1 CO close to hcp and 3 close to fcc sites; a second configuration is somehow complementary, with 1 CO close to fcc and 3 close to hcp sites; a third configuration shows 2 CO close to hcp and 2 close to fcc sites. In summary, for CO intercalated at Gr/Ni(111), we did not find stable configurations including top sites, at variance with what we found in the absence of Gr capping for 0.14 ML and 0.50 ML and proposed in Ref. [14] also for other coverages, but always without Gr. The CO intercalated molecules occupy mainly positions between hollow and bridge sites, and the Gr cover inhibits the occupation of top sites, as suggested in Ref. [22].

3.3. Energetics

Insights about the mutual interaction between Gr, CO molecules and Ni substrate can be inferred from the energetics. The total energy $E_{Gr/CO/Ni}$ of the Gr/CO/Ni(111) system can be split into different contributions. In particular, we can gain information about the stability of the system from the binding energy of intercalated CO at Gr/Ni interface per CO molecule, defined as:

$$E_{interc\ CO} = \frac{1}{N_{CO}} \left(E_{Gr/CO/Ni} - E_{Gr/Ni} - N_{CO} * E_{CO}\right)$$

where $E_{Gr/Ni}$ is the total energy of the corresponding system in absence of intercalated CO, E_{CO} is the total energy of the CO molecule in the gas phase, and N_{CO} the number of intercalated CO molecules. Although it is simply a global energy balance, obtained by comparing different systems and with no information about kinetics barriers, it is interesting to compare $E_{interc\ CO}$ with the corresponding energy quantity without Gr capping, i.e. $E_{ads\ CO}$. As reported in Table S1, for the most stable configurations we found $E_{interc\ CO}$ = −0.34 eV, −1.78 eV, −1.76 eVand $E_{ads\ CO}$ = −2.24 eV, −2.26 eV, −2.15 eV at 0.14 ML, 0.50 ML, and 0.57 ML, respectively. The large variation obtained in between the low and high coverage cannot be attributed to a major difference in the CO–Ni binding, but rather to the different balance between the energy necessary to detach Gr from Ni, which is always the same per C atom, and the energy gained when binding the intercalated CO to the Ni surface, which depends on the coverage [23]. Remarkably, the CO intercalation is always energetically convenient in the coverage range explored.

The adhesion energy of graphene to the CO interlayer can be obtained as:

$$E_{adh\ Gr/(CO/Ni)} = \frac{1}{N_{Gr}} \left(E_{Gr/CO/Ni} - E_{CO/Ni} - E_{Gr}\right)$$

where $E_{CO/Ni}$ is the energy of the corresponding system without Gr capping, E_{Gr} is the energy of the free-standing Gr layer and $N_{Gr}$is the number of C atoms of Gr. Since $E_{adh\ Gr/(CO/Ni)}$ evaluates the interaction of Gr with the substrate, mediated by CO, it is instructive to compare it with the adhesion energy of Gr to the Ni surface without intercalated CO:

$$E_{adh\ Gr/Ni} = \frac{1}{N_{Gr}} \left(E_{Gr/Ni} - E_{Ni} - E_{Gr}\right)$$

where $E_{Gr/Ni}$ is the total energy of the system and E_{Ni} is the energy of the Ni(111) slab. We found $E_{adh\ Gr/(CO/Ni)}$ = −0.05 eV and $E_{adh\ Gr/Ni}$ = −0.16 eV for all CO coverages, indicating that Gr is less bound to CO/Ni than to the clean Ni surface.

In summary, these energy values suggest that at all investigated coverages CO intercalation facilitates the detachment of Gr from Ni.

3.4. Electronic properties

3.4.1. Core-level shifts

We calculated the core-level shifts (CLSs) of the C 1s level (both for C atoms in Gr and in the intercalated CO molecules) for all the configurations considered here, comparing them with those computed for free standing Gr and for Gr directly supported on Ni(111) (Fig. 2). In the latter case, we obtained an average CLS of about 0.4 eV towards higher binding energies (BE) with respect to free standing Gr, with the CLS of C 1s in top and fcc sites differing by about 0.1 eV, well beyond the numerical accuracy of the method (smaller CLS for C in fcc). The effect of the CO intercalation on the C 1s of Gr is strongly dependent on coverage: small for θ = 0.14 ML with respect to free standing Gr, but large for θ = 0.50 ML (with a CLS of about 0.55 eV towards lower BE with respect to free standing Gr) and θ = 0.57 ML (CLS of 0.35 eV), notwithstanding the extremely weak interaction between Gr and CO (see Fig. S7 and Table S2 for details).

As mentioned above, through DFT calculations, we have also access to the CLSs of the C atoms belonging to the intercalated CO molecules. In all cases, those C 1s levels are shifted toward higher BE with respect to what computed for free standing Gr, with CLSs comparable or even larger than those obtained for Gr directly interacting with Ni.

In details, CO molecules forced at 0.14 ML in high symmetry top and bridge sites show the largest C 1s CLSs, namely 1.3 eV in top and 0.75 eV in bridge with respect to free standing Gr. In all the other cases, and for the entire range of investigated coverages, when the CO molecules are precisely in highly symmetric hollow sites (for 0.14 ML) or slightly displaced towards "hybrid" hollow-bridge positions (for 0.50 and 0.57 ML), the CLSs are almost identical and displaced by about 0.55 eV with respect to free standing Gr, i.e. only about 0.1 eV larger than Gr directly interacting with Ni. For comparison, we have calculated also the CLS for CO molecules adsorbed on the bare Ni surface without Gr capping, noticing that in general the presence of Gr does not affect the CO C 1s binding energies.

Fig. 2 reports the calculated CLSs together with the experimental spectra. Since the *ex situ* spectrum was acquired from a region mainly occupied by the 0.50 ML CO structure, with few co-existing 0.57 ML domains, we used the values calculated for 0.50 ML, although those for 0.57 ML are very similar (Fig. S7). For completeness, in Table S2 we also report the values calculated for CO kept fixed in top and in bridge positions at 0.14 ML. First, we observe a good agreement between the theoretical values and the attribution of the experimental peaks concerning the C 1s level of Gr in the different configurations considered (free standing, directly interacting with Ni, detached from Ni by CO intercalation) indicated respectively with violet, green and orange bars.

Moving to the high BE region, the XPS broad component at 285.3 eV (red/blue component in Fig. 2) well matches the calculated values for CO in hollow - both fcc and hcp - and bridge sites (light blue and red bars, respectively). At even higher binding energies, the top site CO peak, predicted to be present at 285.7 eV on the clean Ni surface and absent under the Gr capping at high CO coverage, is almost negligible (black component at ~285.9 eV), with a small residual intensity likely due to defect sites. We include also the calculated C 1s peak of carbide: since the C atoms in the carbide layer on Ni(111) occupy different inequivalent positions, two different values are predicted, one of which is 0.4 eV higher than the one closer to the experimentally attributed value. Further details concerning the DFT calculations for carbide can be found in Ref. [40].

3.4.2. Electronic structure analysis

In Fig. 3a–d we report the band structures projected on the Gr layer for Gr/Ni(111) and for the three investigated Gr/CO/Ni(111) systems (corresponding to 0.14 ML, 0.50 ML and 0.57 ML CO coverages, respectively), whose ball-and-stick representations are shown in Fig. 3e–h. The band structure has been evaluated along the Γ → M → K → Γ and Γ → X → S → Y → Γ high-symmetry paths for the $(\sqrt{7} \times \sqrt{7})$ R19.1° and $\left(2 \times \sqrt{3}\right)$ cell models, respectively (see Fig. S8 for the paths). Only for the 0.14 ML case, the Gr band structure appears to be just slightly hybridized with the Ni metal underneath, in the energy range between −6/−7 eV. For the other two CO coverages, the decoupling from the metal substrate is complete. However, in all three cases we can observe a clear shift of the Dirac cone above the Fermi level, suggesting a net p-type doping effect that increases with the increasing number of intercalated CO molecules. We recall that Gr/Ni(111) is a n-type system, as clearly visible from Fig. 3a and Fig. S13, where, notwithstanding the strong hybridization with the d Ni states, a main feature resembling a linear dispersion crossing can be recognized at about 4 eV below the Fermi level for the spin up C states (Fig. 3a) and at about 3.3 eV for the spin down C states, in reasonable agreement with the feature experimentally detected at 2.66 eV [26]. Therefore, the presence of intercalated CO molecules has a strong and opposite effect on the Gr doping.

The modification of the band structure due to doping affects also the UPS spectra shown in Fig. S12, where the strong shift observed in the π resonance, which moves from about −10 eV to about −7 eV, can be associated to the bands present between 7 eV and 6 eV below Fermi in the calculated bands at Γ (Fig. 3b–d), shifting towards Fermi when the CO coverage increases from 0.14 to 0.57 ML and likely originating from the band at −10 eV before CO intercalation (Fig. 3a).

We further investigated the doping effect by analysing the density of states (DOS) projected on the C atoms of the Gr layer for the three different coverages discussed above: 0.14 ML (blue), 0.50 ML (green), 0.57 ML (red), in Fig. 4a. The zero of the energy scale is set to the

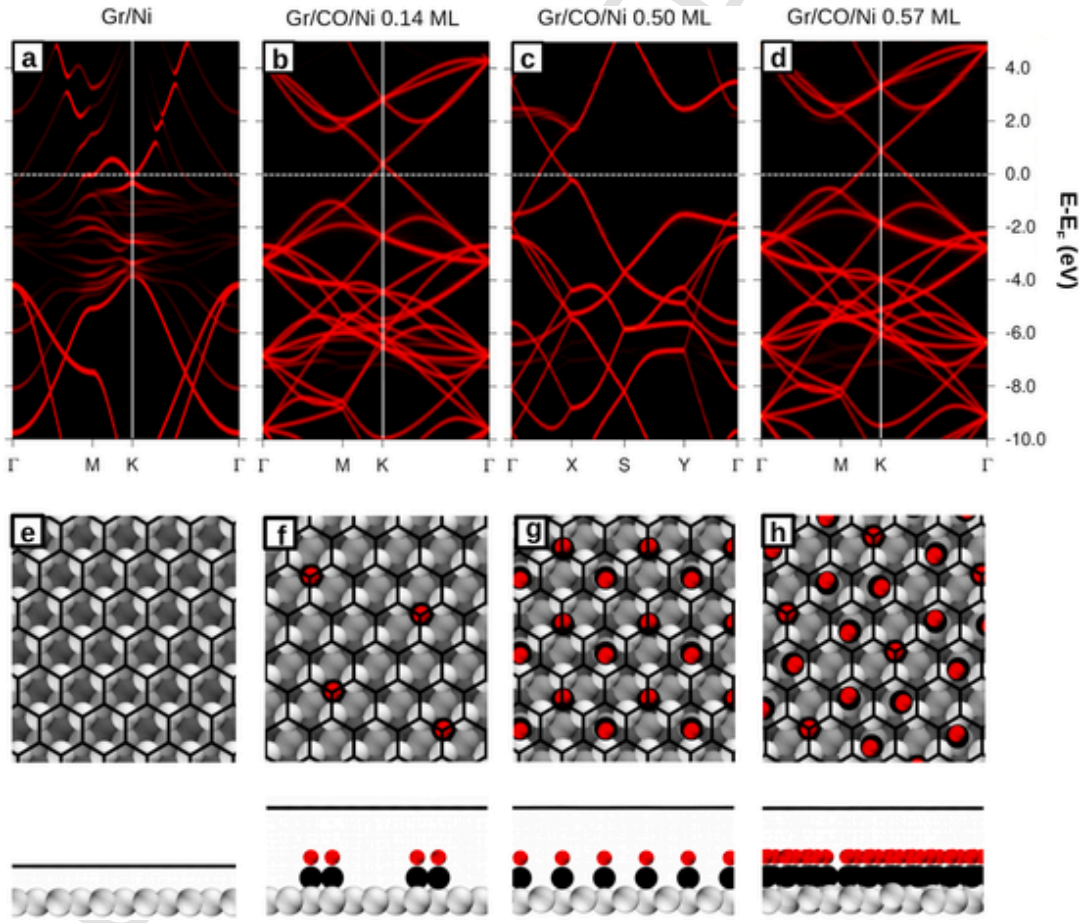

Fig. 3. First row: Gr-projected band structure along the high symmetry path for (a) Gr/Ni and for Gr/CO/Ni at different CO coverages: (b) 0.14 ML, (c) 0.50 ML, and (d) 0.57 ML. The Γ→M→K→Γ and Γ→X→S→Y→ Γ high symmetry paths were used for hexagonal (b and d) and orthorhombic cells (c), respectively (see Fig. S8). The colour scale refers to the value (states (eV)) of the projected DOS. All energies are referred to the corresponding Fermi energy of each system, as indicated by a dashed white line. Second row: Top and side views of representative optimized models for (e) Gr/Ni and for Gr/CO/Ni at different CO coverages: (f) 0.14 ML, (g) 0.50 ML, and (h) 0.57 ML; the side views are taken in a bottom-up direction with respect to the top view panels. Oxygen: red; Carbon: black (wireframe for Gr, spheres in CO); Ni: grey, from light to dark according to the depth from the surface. To simplify the pictures, only the band structure of the majority spin channel for Gr/Ni is reported here. A complete description can be found in Fig. S13. (A colour version of this figure can be viewed online.)

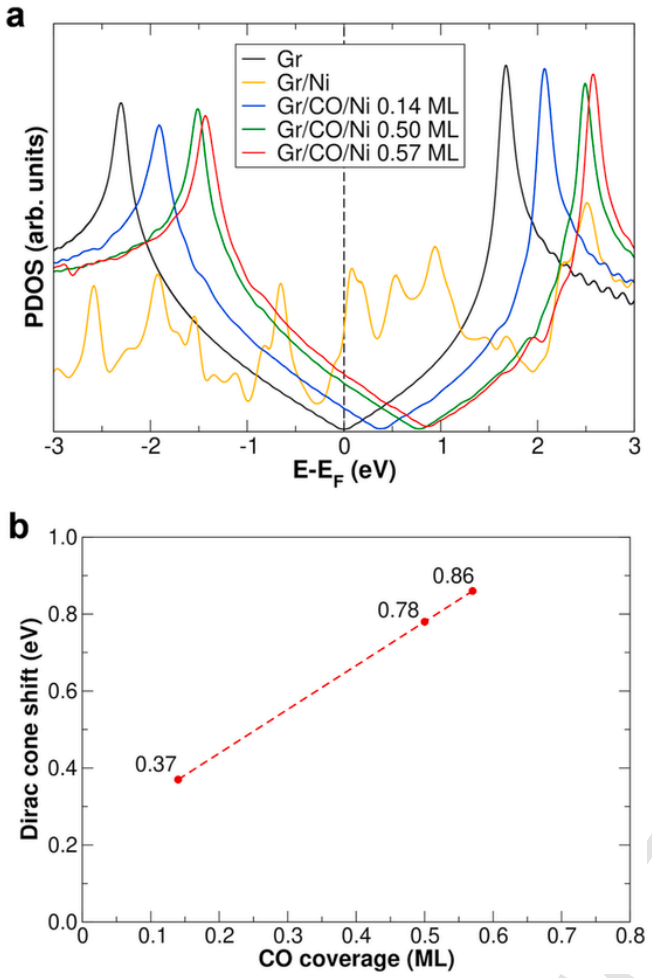

Fig. 4. (a) Projected density of states (PDOS) onto the supported-graphene C p_z states for the optimized models of Gr/CO/Ni(111) at different CO coverages (0.14 ML, 0.50 ML, and 0.57 ML). The C p_z PDOS of free-standing graphene and of Gr on Ni without intercalated CO is shown for comparison. The PDOS value for each system is normalized to one C atom of graphene. All energies are referred to the corresponding Fermi energy of each system, as indicated by a dotted black line. (b) Linear relationship of the shift of the Dirac cone with respect to the Fermi energy for Gr/CO/Ni(111) (in eV) vs. the CO coverage. (A colour version of this figure can be viewed online.)

Fermi energy of the free standing case. The plot clearly shows that the DOS of Gr, detached from the substrate by intercalated CO, recovers its free-standing typical shape, but with a rigid shift towards higher energies, in perfect agreement with the projected band structures shown in Fig. 3. The result, irrespective of the particular CO adsorption sites, is a sizeable p-doping effect, monotonically and linearly increasing with the CO coverage up to 0.86 eV at the saturation value (see Fig. 4b). Similar results have been obtained by Grånäs et al. [7] for Ir(111)-supported Gr: also in that case the CO intercalation (Gr/CO/Ir(111)) makes the Gr electronic properties very similar to free standing Gr but with a sizeable p-doping effect (a Fermi energy shift of about 0.6 eV). However, there is an important difference between the two substrates. Even in the absence of CO intercalation, Ir(111)-supported Gr (Gr/Ir(111)) is a weakly interacting system and shows a slight p-doping. At variance, Gr directly supported on Ni(111) (Gr/Ni(111)) is a strongly interacting n-type system, whereas even low amounts of intercalated CO molecules (0.14 ML) turn Gr/CO/Ni(111) into a p-type system. We thus conclude that a clear inversion in the doping of the Ni(111) supported Gr layer is observed before and after CO intercalation. The more the intercalated CO molecules, the stronger the p-type doping effect. We expect that the electron density lost by Gr has been transferred to the underlying CO molecules, which are strong Lewis acids and, thus, excellent electron acceptors. This will be verified in the next section on the basis of differential electron density maps and of CO molecular descriptors, such as CO bond length and stretching frequency.

Finally, we summarize and compare all our DFT results, as a function of the CO coverage, for: i) the position of the Gr π band bottom at Γ; ii) the Gr doping, measured in terms of the shift of the Dirac cone from the Fermi energy of free Gr, and iii) Gr C 1s CLS. We found a strong correlation between the calculated quantities, in particular between the shifts of the Gr π band bottom at Γ and of the Dirac cone, as can be seen in Fig. S14 (the zero level corresponds to the free Gr). Similar findings have been reported in Ref. [41] although for a rather different system (defected Gr doped with nitrogen substitutional to carbon atoms or with pyridinic nitrogen at vacancies edges). Our results show that p-doping corresponds to negative C 1s CLS, in line with a rigid band model and the results for intercalated structures of Gr on Ir(111) [42,43]. The correlation between the Gr doping and the C 1s CLS, however, shows deviations from that simple model. In Ref. [43] similar deviations have been attributed to charge transfer effects.

3.4.3. Electronic charge transfer analysis and molecular descriptors

Similarly to what done for the energy, we can split the electron density into different contributions and then plot their difference with respect to the electron distribution of the whole system, Gr/CO/Ni. Fig. S9 shows the contour plots of the differential electron density calculated in two different ways:

$$\Delta n_1(\boldsymbol{r}) = n_{Gr/CO/Ni}(\boldsymbol{r}) - n_{Gr}(\boldsymbol{r}) - n_{CO}(\boldsymbol{r}) - n_{Ni}(\boldsymbol{r})$$

and

$$\Delta n_2(\boldsymbol{r}) = n_{Gr/CO/Ni}(\boldsymbol{r}) - n_{Gr}(\boldsymbol{r}) - n_{CO/Ni}(\boldsymbol{r})$$

The first plot highlights the large polarization of the CO molecules due to the adsorption on Ni. In the second plot, the interaction between Gr and the intercalated CO is magnified, and a very small electron transfer from Gr to CO is visible. The latter can be quantified calculating the Löwdin charges [39]: C atoms of Gr give on average to the intercalated CO 0.004, 0.018 and 0.022 electrons for coverage of 0.14 ML, 0.50 ML and 0.57 ML, respectively, following an almost linear trend. We notice that this electron transfer, although very small, has a direction compatible with the p-doping effect found in the projected DOS analysis.

In order to establish whether the electron density loss of the Gr layer observed upon CO intercalation is due to an electronic charge transfer to the underlying adsorbed CO molecules, we have investigated two molecular descriptors, which are the CO bond length and the CO stretching frequency, as reported in detail in Tables S3, S4 and S5 of the Supplementary Data for CO coverages of 0.14 ML, 0.50 ML and 0.57 ML, respectively. First of all, we observe that, at all three CO coverages, the presence of the Gr layer over the CO molecules adsorbed on the Ni(111) surface causes an elongation of the CO bond length (by 0.1 Å) and a corresponding decrease of the CO stretching frequency. These descriptors indicate that electron density is transferred to the CO π* states. This electron density comes probably not only from Gr but partly also from the Ni surface. We may notice that CO molecules on different adsorption sites (fcc or hcp) behave differently. When comparing the behaviour at different coverages, we notice that the CO stretching frequency shift is a more sensitive descriptor than the bond length, with a stronger variation observed for the higher coverages (0.50 and 0.57 ML) with respect to the case of low coverage (0.14 ML).

4. Conclusions

In summary, performing a joint experimental/theoretical investigation of the Gr/Ni(111) with intercalated CO at the interface, we have shown that CO exposures in the mbar regime lead to Gr delamination,

with the CO molecules forming an ordered array at the Gr/Ni(111) interface. We found that for CO coverages ≥0.14 ML Gr is decoupled from the substrate and recovers the main peculiar electronic features of the free-standing case, both in the simulated STM images and in the shape of the DOS. DFT simulations provide atomic-scale adsorption patterns, which for high coverages (0.50 ML and 0.57 ML) are characterized by molecules mainly in hollow fcc and hcp sites, but slightly displaced towards bridge positions. This is compatible with a deconvolution of the C 1s XPS signal into the corresponding components, with BE in a range close to that characteristic of Gr interacting with Ni. However, the major effect of the CO intercalation on the C 1s XPS signal is a large contribution towards smaller BE of the decoupled Gr, clearly confirmed also by DFT.

Although Gr weakly interacts with the underlying CO/Ni support, losing a very small fraction of electrons (the amount is roughly proportional to the CO coverage and at most equal to a couple of hundredths of electrons per C atom), this originates a sizeable p-doping effect, with a shift of the Fermi level roughly proportional to the coverage, as large as 0.86 eV for 0.57 ML of intercalated CO. Such a high sensitivity of the Gr doped state to the presence of intercalated CO molecules opens the way to the design of new sensors based on the Graphene/Ni(111) interface to easily detect and quantify the presence of this harmful gas.

CRediT authorship contribution statement

Simone Del Puppo: DFT Investigation, Visualization, Writing - original draft. **Virginia Carnevali:** DFT Methodology, Investigation, Writing - review & editing. **Daniele Perilli:** DFT Methodology, Investigation, Validation, Visualization, Writing - original draft. **Francesca Zarabara:** DFT Investigation. **Alberto Lodi Rizzini:** Experimental Investigation, Formal analysis, Writing - review & editing. **Gabriele Fornasier:** Experimental Investigation. **Erik Zupanič:** Experimental Methodology, Investigation, Writing - review & editing. **Sara Fiori:** Experimental analysis, Validation, Visualization, Writing - original draft. **Laerte L. Patera:** Experimental Methodology, Investigation, Writing - review & editing. **Mirco Panighel:** Experimental Validation, Writing - review & editing. **Sunil Bhardwaj:** Experimental Investigation. **Zhiyu Zou:** Experimental Validation, Writing - review & editing. **Giovanni Comelli:** Supervision, Writing - review & editing. **Cristina Africh:** Funding acquisition, Conceptualization, Supervision, Visualization, Writing - review & editing. **Cinzia Cepek:** Conceptualization, Supervision, Formal analysis, Visualization, Writing - review & editing. **Cristiana Di Valentin:** Conceptualization, Supervision, Funding acquisition, Visualization, Writing - original draft. **Maria Peressi:** Conceptualization, Supervision, Funding acquisition, Visualization, Writing - original draft.

Declaration of competing interest

The authors declare that they have no known competing financial interests or personal relationships that could have appeared to influence the work reported in this paper.

Acknowledgments

We acknowledge financial support from Italian Ministry of Foreign Affairs and International Cooperation (Executive Programme with Serbia 2019–2021 – "Progetti di Grande Rilevanza") and from University of Trieste (program "Finanziamento di Ateneo per progetti di ricerca scientifica – FRA 2018"). We thank Željko Šljivančanin for fruitful discussions. Computational resources have been obtained from CINECA through the ISCRA initiative and the agreement with the University of Trieste.

E.Z. acknowledges support from the Slovenian Research Agency (ARRS), Core Research Funding No. P1-0099. Z.Z. and S.B. acknowledge support by the "ICTP TRIL Programme, Trieste, Italy" in the framework of the agreement with CNR-IOM. This work has been supported by the project "MADAM - Metal Activated 2D cArbon-based platforMs" funded by the MIUR Progetti di Ricerca di Rilevante Interesse Nazionale (PRIN) Bando 2017 - grant 2017NYPHN8.

Appendix. Supplementary data

Supplementary data to this article can be found online at https://doi.org/10.1016/j.carbon.2021.01.120.

References

[1] L. Bignardi, P. Lacovig, M.M. Dalmiglio, F. Orlando, A. Ghafari, L. Petaccia, A. Baraldi, R. Larciprete, S. Lizzit, Key role of rotated domains in oxygen intercalation at graphene on Ni(111), 2D Mater. 4 (2017) 025106.
[2] A. Varykhalov, J. Sanchez-Barriga, A.M. Shikin, C. Biswas, E. Vescovo, A. Rybkin, D. Marchenko, O. Rader, Electronic and magnetic properties of quasifreestanding graphene on Ni, Phys. Rev. Lett. 101 (2008) 157601.
[3] S.L. Wong, H. Huang, Y. Wang, L. Cao, D. Qi, I. Santoso, W. Chen, A.T.S. Wee, Quasi-free-standing epitaxial graphene on SiC (0001) by fluorine intercalation from a molecular source, ACS Nano 5 (2011) 7662–7668.
[4] P. Sutter, J.T. Sadowski, E.A. Sutter, Chemistry under cover: tuning metal-graphene interaction by reactive intercalation, J. Am. Chem. Soc. 132 (2010) 8175–8179.
[5] R. Larciprete, S. Ulstrup, P. Lacovig, M. Dalmiglio, M. Bianchi, F. Mazzola, L. Hornekær, F. Orlando, A. Baraldi, P. Hofmann, S. Lizzit, Oxygen switching of the epitaxial graphene–metal interaction, ACS Nano 6 (2012) 9551–9558.
[6] R. Mu, Q. Fu, Q.; L. Jin, L. Yu, G. Fang, D. Tan, X. Bao, visualizing chemical reactions confined under graphene, in: Angew Chem Int (Ed.), 51, 2012, pp. 4856–4859.
[7] E. Grånäs, M. Andersen, M.A. Arman, T. Gerber, B. Hammer, J. Schnadt, J.N. Andersen, T. Michely, J. Knudsen, CO intercalation of graphene on Ir (111) in the millibar regime, J. Phys. Chem. C 117 (2013) 16438–16447.
[8] V. Shah, T. Li, K.L. Baumert, H. Cheng, D.S. Sholl, A comparative study of CO chemisorption on flat and stepped Ni surfaces using density functional theory, Surf. Sci. 537 (2003) 217–227.
[9] X. Hao, B. Wang, Q. Wang, R. Zhang, D. Lib, Insight into both coverage and surface structure dependent CO adsorption and activation on different Ni surfaces from DFT and atomistic thermodynamics, Phys. Chem. Chem. Phys. 18 (2016) 17606–17618.
[10] J.C. Campuzano, R. Dus, G. Greenler, The sticking probability, dipole moment and absolute coverage of CO on Ni(111), Surf. Sci. 102 (1981) 172–184.
[11] L. Becker, S. Aminipirooz, B. Hillert, M. Pedio, J. Haase, Threefold-coordinated hollow adsorption site for Ni(111)-c(4x2)-CO: a surface-extended x-ray absorption fine structure study, Phys. Rev. B 47 (1993) 9710–9714.
[12] L.D. Mapledoram, M.P. Bessent, A. Wander, D.A. King, An automated tensor LEED analysis of the Ni(111) c(4x2)-2CO structure, Chem. Phys. Lett. 228 (1994) 527–532.
[13] P.T. Sprunger, F. Besenbacher, I. Stensgaard, STM investigation of the Ni(111)-c(4x2)-2CO structure, Chem. Phys. Lett. 243 (1995) 439–444.
[14] A. Eichler, CO adsorption on Ni(111) – a density functional theory study, Surf. Sci. 526 (2003) 332–340.
[15] M.E. Davila, M.C. Asensio, D.P. Woodruff, K.-M. Schindler, Ph. Hofmann, K.-U. Weiss, R. Dippel, P. Gardner, V. Fritzsche, A.M. Bradshaw, J.C. Conesa, A.R. González-Elipe, Structure determination of Ni(111) c(4 × 2)-CO and its implications for the interpretation of vibrational spectroscopic data, Surf. Sci. 311 (1994) 337–348.
[16] N. Ikemiya, T. Suzuki, M. Ito, Adlayer structures of CO adsorbed on Ni(111) electrode surfaces studied by in situ STM combined with IRAS, Surf. Sci. 466 (2000) 119–126.
[17] A. Bandara, S. Katano, J. Kubota, K. Onda, A. Wada, K. Domen, C. Hirose, The effect of co-adsorption of on-top CO on the sum-frequency generation signal of bridge CO on the Ni(111) surface, Chem. Phys. Lett. 290 (1998) 261–267.
[18] A. Beniya, N. Isomura, H. Hirata, Y. Watanabe, Low temperature adsorption and site-conversion process of CO on the Ni(111) surface, Surf. Sci. 606 (2012) 1830–1836.
[19] W. Erley, K. Besocke, H. Wagner, Absolute coverage determination of CO on Ni(111), J. Chem. Phys. 66 (1976) 5269–5273.
[20] G. Held, J. Schuler, W. Sklarek, H.P. Steinruck, Determination of adsorption sites of pure and coadsorbed CO on Ni(111) by high resolution X-ray photoelectron spectroscopy, Surf. Sci. 398 (1998) 154–171.
[21] W. Braun H.P. Steinruck G. Held The surface geometries of the medium and high coverage carbon monoxide structures c(2x4)–2CO and $p\left(\sqrt{7}\times\sqrt{7}\right)R19^{o}$ –4CO on Ni(111) Surf. Sci. 575 2005 343 357
[22] M. Wei, Q. Fu, Y. Yang, W. Wei, E. Crumlin, H. Bluhm, X. Bao, Modulation of surface chemistry of CO on Ni(111) by surface graphene and carbidic carbon, J. Phys. Chem. C 119 (2015) 13590–13597.
[23] D. Perilli, S. Fiori, M. Panighel, H. Liu, C. Cepek, M. Peressi, G. Comelli, C. Africh, C. Di Valentin, Mechanism of CO intercalation through the graphene/

Ni(111) interface and effect of doping, J. Phys. Chem. Lett. 11 (2020) 8887–8892.
[24] D. Nečas, P. Klapetek, Gwyddion: an open-source software for SPM data analysis, Cent. Eur. J. Phys. 10 (2012) 181–188 Code available from http://Gwyddion.net/.
[25] L.L. Patera, C. Africh, R.S. Weatherup, R. Blume, S. Bhardwaj, C. Castellarin-Cudia, A. Knop-Gericke, R. Schloegl, G. Comelli, S. Hofmann, C. Cepek, *In situ* observations of the atomistic mechanisms of Ni catalyzed low temperature graphene growth, ACS Nano 7 (2013) 7901–7912.
[26] C. Africh, C. Cepek, L.L. Patera, G. Zamborlini, P. Genoni, T.O. Menteş, A. Sala, A. Locatelli, G. Comelli, Switchable graphene-substrate coupling through formation/dissolution of an intercalated Ni-carbide layer, Sci. Rep. 6 (2016) 19734.
[27] P. Giannozzi et al. Quantum Espresso: a modular and open-source software project for Quantum simulations of materials, J. Phys.: cond. MatterCode available fromhttp://www.quantum-espresso.org/200921
[28] J.P. Perdew, K. Burke, M. Ernzerhof, Generalized gradient approximation made simple, Phys. Rev. Lett. 77 (1996) 3865–3868.
[29] Pseudopotentials available onhttps://www.quantum-espresso.org/pseudopotentials
[30] S. Grimme, Density functional theory with London dispersion corrections, Wiley Interdisciplinary Reviews: Computational Molecular Science 1 (2011) 211–228.
[31] F. Bianchini, L.L. Patera, M. Peressi, C. Africh, G. Comelli, Atomic scale identification of coexisting graphene structures on Ni(111), J. Phys. Chem. Lett. 5 (2014) 467–473.
[32] H.J. Monkhorst, J.D. Pack, Special points for Brillouin-zone integrations, Phys. Rev. B 13 (1976) 5188–5192.
[33] M. Methfessel, A.T. Paxton, High-precision sampling for Brillouin-zone integration in metals, Phys. Rev. B 40 (1989) 3616–3621.
[34] E. Pehlke, M. Scheffler, Evidence for site-sensitive screening of core holes at the Si and Ge (001) surface, Phys. Rev. Lett. 71 (1993) 2338–2341.
[35] J.N. Andersen, D. Hennig, E. Lundgren, M. Methfessel, R. Nyholm, M. Scheffler, Surface core-level shifts of some 4*d*-metal single-crystal surfaces: experiments and *ab initio* calculations, Phys. Rev. B 50 (1994) 17525–17533.
[36] A. Kokalj, J. Mol. Graph. Model. 17 (1999) 176–179 Code available from http://www.xcrysden.org/.
[37] W. Humphrey, A. Dalke, K. Schulten, VMD: Visual Molecular Dynamics, J. Mol. Graph. 14 (1996) 33–38.
[38] J. Tersoff, D.R. Hamann, Theory of the scanning tunneling microscope, Phys. Rev. B 31 (1985) 805–813.
[39] P.O. Löwdin, Quantum theory of many-particle systems. I. Physical interpretations by means of density matrices, natural spin-orbitals, and convergence problems in the method of configurational interaction, Phys. Rev. 97 (1955) 1474–1489.
[40] S. Stavrić, S. Del Puppo, Ž. Šljivančanin, M. Peressi, First-principles Study of Nickel Reactivity under Two-Dimensional Cover: Ni2C formation at rotated graphene/Ni(111) interface, Phys. Rev. Materials 5 (2021) 014003.
[41] R.J. Koch, M. Weser, W. Zhao, F. Viñes, K. Gotterbarm, S.M. Kozlov, O. Höfert, M. Ostler, C. Papp, J. Gebhardt, H.-P. Steinrück, A. Görling, Th. Seyller, Growth and electronic structure of nitrogen-doped graphene on Ni(111), Phys. Rev. B 86 (2012) 07540.
[42] M. Andersen, L. Hornekær, B. Hammer, Understanding intercalation structures formed under graphene on Ir(111), Phys. Rev. B 90 (2014) 155428.
[43] U.A. Schröder, M. Petrović, T. Gerber, A.J. Martínez Galera, E. Grånäs, M.A. Arman, C. Herbig, J. Schnadt, M. Kralj, J. Knudsen, T. Michely, Core level shifts of intercalated graphene, 2D Mater. 4 (2017) 015013.